Applied Catalysis B: Environmental 111–112 (2012) 389–396

Contents lists available at SciVerse ScienceDirect

Applied Catalysis B: Environmental

journal homepage: www.elsevier.com/locate/apcatb

Improvement of photocatalytic activity of TiO_2 nanoparticles on selectively reconstructed layered double hydroxide

Ruijuan Lu, Xin Xu, Jiapeng Chang, Yue Zhu, Sailong Xu, Fazhi Zhang*

State Key Laboratory of Chemical Resource Engineering, Beijing University of Chemical Technology, Beijing 100029, China

ARTICLE INFO

Article history:
Received 31 July 2011
Received in revised form 11 October 2011
Accepted 16 October 2011
Available online 20 October 2011

Keywords:
TiO_2
Photocatalysis
Layered double hydroxide
Junction
Doping

ABSTRACT

Supported TiO_2 nanoparticles have been successfully fabricated by selective reconstruction of a Cu^{2+}, Mg^{2+}, Al^{3+}, Ti^{4+}-containing layered double hydroxide (CuMgAlTi-LDH) precursor, synthesized by coprecipitation, through calcination and rehydration process. A systematic investigation of the structural characterization and the photodegradation tests of methylene blue (MB) dye molecules from solution under both UV and visible light irradiation for the resulting TiO_2/CuMgAl-RLDH sample were carried out. Anatase-type TiO_2 nanoparticles are found to be homogeneously distributed on the surface of the selectively reconstructed CuMgAl-RLDH support. And the direct evidence for the surface TiO_2/LDH heterojunction formed on CuMgAl-RLDH is presented. For MB photodegradation under UV light or visible light illumination, TiO_2/CuMgAl-RLDH sample has superior photocatalytic properties to the rehydrated single phase R-TiO_2, the physical mixture of R-TiO_2 and CuMgAl-RLDH, the composite CuTi/MgAl-RLDH synthesized by the rehydration of mixture of MgAl-MMO and CuTi-MMO, and the TiO_2/MgAl-RLDH prepared under the same procedure as TiO_2/CuMgAl-RLDH without containing Cu ions. The skeleton Cu^{2+} ions dispersed in the mainlayer of CuMgAl-RLDH support can enable the photocatalytic activity for MB photodegradation. The TiO_2/LDH heterojunction nanostructure is proposed to contribute the efficient spatial separation between the photogenerated electrons and holes, which can concomitantly improve the photocatalytic activity. Our method provides a novel approach to fabricate new modes of load-type doped semiconductor photocatalysts which are both active under illumination by UV and visible light.

1. Introduction

Semiconducting photocatalysts have attracted extensive attention due to their potential industrial applications such as environmental purification and solar energy cell [1–4]. Although the remarkable progress has been made in the synthesis of new types of photocatalysts working in the ultraviolet or visible light regions, titanium dioxide-based semiconductor materials are still considered to be one of the superior candidates for their many desirable properties. Taking into account the large band gap of TiO_2 semiconductor, which requires UV light for excitation and thus limits the efficient utilization of solar energy, the improving of photoefficiency of the electronic process as well as the extending of absorption into the visible part of the spectrum plays an important role for the technical applications of TiO_2 in the future [5].

The use of supported TiO_2 has allowed the enhancement of photocatalysis rates in comparison with neat TiO_2. Active carbon [6] and molecular sieves [7,8] have been reported to be adopted as the supports. It was shown that such arrangements (highly adsorptive supports and nanosized TiO_2) produced higher quantum yields. Reddy et al. [9] attempted to use a transition metal modified MCM-41 for supporting TiO_2 and found that some metals, such as Cu and Cr, can enhance the performance of the photocatalysts. However, because the supported particulate catalysts are hard to be homogeneously dispersed and unstable during the course of photocatalytic reactions, it is possible to lead to the reduced photocatalytic activity and lost in the reaction to a great extent. Development of new approach for preparation of supported TiO_2-based photocatalysts with improved activity and stability working in visible light region is thus highly valued.

As one member of clay family, layered double hydroxides (LDHs, also known as hydrotalcite-like materials) are one such potential inorganic support. They can be described by the general formula $[M_{1-x}^{2+}M_x^{3+}(OH)_2]^{x+}A^{n-}_{x/n}\cdot mH_2O$, where M^{2+} and M^{3+} are di-and tri-valent cations, respectively; the value of the coefficient x is equal to the molar ratio of $M^{3+}/(M^{2+}+M^{3+})$; and A^{n-} is an anion [10–12]. This flexibility in composition allows LDHs with a wide variety of properties to be prepared [13]. One of the most attractive features of LDHs materials is the so called "reconstruction effect" [14]: calcination of MgAl-LDH at moderate temperatures leads to the formation of magnesium aluminum mixed metal oxides (MMO), and rehydration of MMO results in spontaneous structural reconstruction of

* Corresponding author. Fax: +86 10 6442 5385.
E-mail address: zhangfz@mail.buct.edu.cn (F. Zhang).

0926-3373/$ – see front matter © 2011 Elsevier B.V. All rights reserved.
doi:10.1016/j.apcatb.2011.10.022

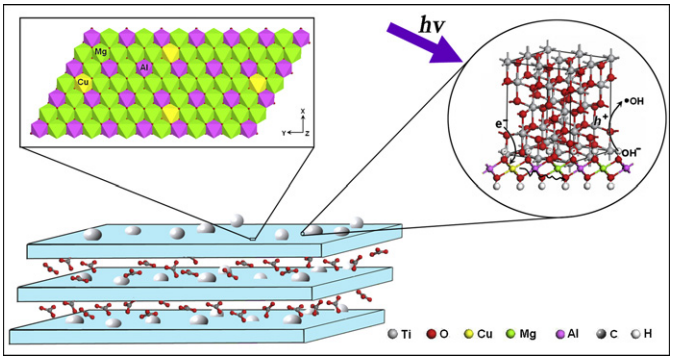

Fig. 1. Schematic illustration of the resulting TiO_2/CuMgAl-RLDH sample and the proposed photocatalytic mechanism.

LDH. The reconstructed LDHs have been reported to be used as solid base catalysts [15], for sensing water uptake in organic coatings [16], and even for fabrication of erasable nanoporous antireflection coatings [17].

In the present work, by taking advantage of the characteristic "reconstruction effect" of LDH materials, we describe the fabrication of surface-doped TiO_2 semiconductor supported on LDH with high dispersion. Cu^{2+}, Mg^{2+}, Al^{3+}, Ti^{4+}-containing LDH was first synthesized by coprecipitation. Then, CuMgAlTi-MMO was obtained after calcination of the LDH precursor in air at 400 °C. By subsequent rehydration in deionized water at room temperature, LDH structure with Cu^{2+}, Mg^{2+}, Al^{3+} in mainlayers (CuMgAl-RLDH) was selectively reconstructed producing the TiO_2 nanoparticles supported on the LDH surface (Fig. 1). Substituting part magnesium with copper ions in the framework during synthesis of LDH makes it possible to improve the photoefficiency. The resulting samples were characterized by X-ray diffraction (XRD), Fourier transform infrared spectroscopy (FT-IR), ultraviolet–visible spectroscopy (UV–vis), scanning electron microscopy (SEM), transmission electron microscopy (TEM), X-ray photoelectron spectroscopy (XPS), and electron paramagnetic resonance spectroscopy (EPR). The photocatalytic performance of the resulting sample was investigated using the degradation of MB dye molecules under both UV and visible light irradiation as a probe reaction. It is demonstrated that the resulting sample exhibit excellent photocatalytic efficiencies.

2. Experimental

2.1. Materials preparation

The carbonate-intercalated CuMgAlTi-LDH precursor was synthesized by the coprecipitation method. All reagents were commercially available and used as received without further purification. For the synthesis of CuMgAlTi-LDH with Cu/Mg/Al/Ti molar ratio of 1/30/10/9, a solution of $Cu(NO_3)_2{\cdot}3H_2O$ (0.002 mol), $Mg(NO_3)_2{\cdot}6H_2O$ (0.06 mol), $Al(NO_3)_3{\cdot}9H_2O$ (0.02 mol), and $TiCl_4$ (0.018 mol) were dissolved in 100 mL of deionized water (solution *A*). NaOH (0.16 mol) and Na_2CO_3 (0.016 mol) were dissolved in 100 mL of deionized water (solution *B*). Solution *B* was added dropwise to solution *A* until a pH of 8.5 was attained, and the system was then aged at 60 °C for 18 h. The solid product was collected by centrifugation, washed with deionized water and alcohol separately, and finally dried at 90 °C overnight. The dried LDH precursor was further calcined in air at 400 °C for 5 h, with a heating rate of 2 °C/min, in order to transform the LDH precursor into CuMgAlTi-MMO. For comparison, samples of MgAl-MMO, CuMgAl-MMO, CuTi-MMO, and MgAlTi-MMO with Mg/Al molar ratios of 3/1, Cu/Mg/Al molar ratios of 1/30/10, Cu/Ti molar ratios of 1/9, and Mg/Al/Ti molar ratios of 30/10/19, respectively, as well as a single metal oxide TiO_2, were synthesized under the same reaction conditions.

The CuMgAlTi-MMO powder (1 g) was placed into 100 mL deionized water, and then stirred for 24 h at room temperature. The resulting TiO_2/CuMgAl-RLDH was collected by centrifugation, washed several times with deionized water, and dried at 60 °C overnight. For comparison, after the rehydration of MgAlTi-MMO under the same conditions we got TiO_2/MgAl-RLDH. CuTi/MgAl-RLDH was synthesized by the rehydration of the mixture of MgAl-MMO and CuTi-MMO. Additionally, R-TiO_2/CuMgAl-RLDH was a mechanical mixture of the rehydrated TiO_2 and rehydrated CuMgAl-MMO (denoted R-TiO_2 and CuMgAl-RLDH, respectively).

2.2. Characterization

XRD patterns of the products were recorded on a Shimadzu XRD-6000 diffractometer, using Cu Kα radiation (λ = 0.15418 nm) at 40 kV and 30 mA. FT-IR spectra were recorded using KBr discs in the region 400–4000 cm^{-1} with a Bruker Vector 22 spectrometer. SEM images were obtained using a Hitachi S-4700 field emission SEM at 20 kV, with the surface of the samples coated with a thin platinum layer to avoid a charging effect. TEM images were recorded on a JEOL JEM-2010 high-resolution transmission electron microscope at an accelerating voltage of 200 kV. The sample was ultrasonically dispersed in ethanol, and then the suspension was deposited on a microgrid coated with a holey carbon film. UV–vis diffuse reflectance spectra were recorded at room temperature in air on a Shimadzu UV-2501PC spectrometer equipped with an integrating sphere attachment using $BaSO_4$ as background. Elemental analyses for metals were performed with a Shimadzu ICPS-7500 inductively coupled plasma emission spectrometer (ICP-ES) on solutions prepared by dissolving the samples in dilute HCl. XPS were recorded with a PHIQ2000 X-ray photoelectron spectrometer equipped with a monochromatized Al Kα X-ray source. An operating power of 25 W was used with a spot diameter of 100 μm. EPR spectra of paramagnetic species were recorded with a Bruker EPR 300E spectrometer, the irradiation source (λ = 355 nm) was a Quanta-Ray Nd:YAG pulsed (10 pulses/s) laser system.

2.3. Photocatalytic activity measurements

Photocatalytic activities of the TiO_2-based samples were evaluated using the photodegradation of MB under UV and visible light irradiation as the model reaction. Under visible light irradiation, a quartz beaker (capacity 150 mL) was used as the photoreaction vessel. Typically, the reaction system containing MB (aqueous solution, 1×10^{-5} M) and catalyst sample (0.3 g/L) was magnetically stirred in the dark for 30 min to reach the adsorption equilibrium of MB with the catalyst and was then exposed to light from a 300 W Xe lamp equipped with a UV cutoff filter (λ ≥ 420 nm). At specific time intervals, 3 mL of the reaction solution was withdrawn by a syringe. The solution was centrifuged to remove the catalyst sample before being analyzed by UV–vis absorption spectroscopy. A blank reaction was carried out under the same reaction conditions without adding any catalyst. For UV light irradiation, the procedure is the same, excepting for using a 500-W high-pressure mercury lamp equipped with a double-walled quartz glass cooling tube and a quartz reactor (capacity 250 mL) as the reaction equipment.

3. Results and discussion

Fig. 2 illustrates the XRD patterns of the samples of carbonate-intercalated CuMgAlTi-LDH precursor, CuMgAlTi-MMO, and TiO_2/CuMgAl-RLDH. The patterns of the LDH precursor exhibit the characteristic reflections of a well-ordered layer structure, with

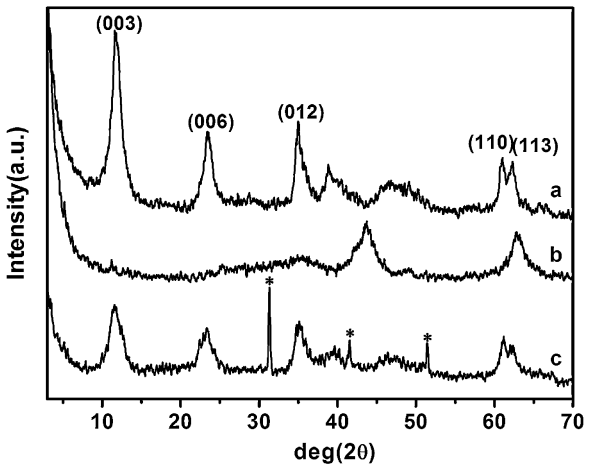

Fig. 2. Powder XRD patterns of (a) CuMgAlTi-LDH, (b) CuMgAlTi-MMO, and (c) TiO_2/CuMgAl-RLDH. (*Indicates the peaks corresponding to anatase-type TiO_2.)

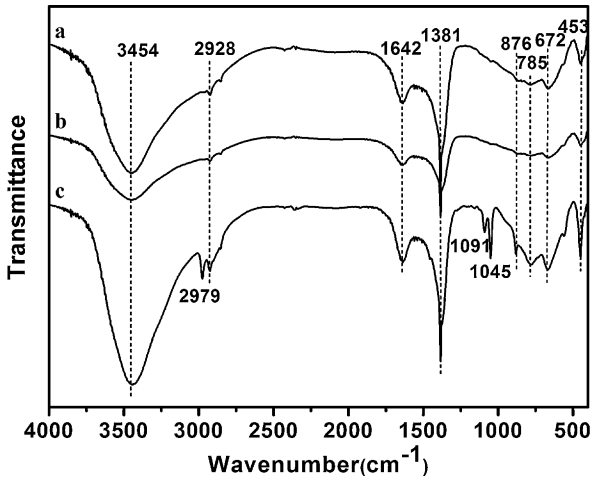

Fig. 3. FT-IR spectra of (a) CuMgAlTi-LDH, (b) CuMgAlTi-MMO, and (c) TiO_2/CuMgAl-RLDH.

a series of (0 0 l) peaks appearing as narrow lines at low angle 2θ and weaker non-basal reflections at higher angles (Fig. 2a). Calcination of the LDH precursor at 400 °C produces the MMO material with rock-salt type (Fig. 2b). After the MMO were soaked in deionized water at room temperature, the original layer structure of LDH was recovered due to the "reconstruction effect". It is worth noting that, besides the characteristic reflections of LDH structure, three reflection peaks at 31.3°, 41.5° and 51.4° appear (Fig. 2c), which are attributed to the anatase-type TiO_2 (JCPDS, No. 84-1750). Additionally, the diffraction peaks of TiO_2 are relatively sharp and intense, indicating the high crystalline character of TiO_2 particles.

The basal spacing of LDH crystal (the distance from the center of one layer to the other one that in the adjacent layer) is determined by the (0 0 3) reflection. The sum of the calculated length of the carbonate (≈2.85 Å) and the layer thickness (≈4.80 Å) is about 7.65 Å, which almost coincides with the d-spacing value of the CuMgAlTi-LDH precursor (7.48 Å, Table 1). This demonstrates that a monolayer of carbonate is oriented perpendicularly to the layers in the interlamellar domain [13]. Table 1 shows that the d-spacing value of CuMgAlTi-LDH is smaller than that of TiO_2/CuMgAl-RLDH (7.82 Å). This can be interpreted by considering that OH groups bonded to TiO_2/CuMgAl-RLDH are less polarized and hence weaker hydrogen bonds may be formed between the OH groups and interlayer carbonate anions. The value of the unit cell parameter a (=$2d_{110}$), is a function of the average cation–cation distance within the layers of LDH. In our case, the value of a remains essentially constant (≈3.04 Å) (Table 1), which represents the closest possible approach of Mg^{2+} and Al^{3+} cations [18]. Table 1 also summarizes the chemical compositions of the three samples. The molar ratios of Cu/Al, Mg/Al, and Ti/Al are essentially identical, suggesting that the calcination and rehydration process did not make the loss of metal elements.

FT-IR spectra of LDH precursor, MMO, and TiO_2/CuMgAl-RLDH are shown in Fig. 3. For the carbonate-intercalated LDH, the broad band at 3454 cm^{-1} corresponds to the O–H stretching vibration of interlayer water molecules and hydroxyl groups in the brucite-like layers. A weak shoulder peak recorded at around 2900 cm^{-1} has been ascribed to the OH stretching mode of interlayer water molecules, hydrogen-bonded to interlayer carbonate anions [19,20]. The band observed at 1642 cm^{-1} is due to O–H banding vibrations of interlayer water molecules. The sharp and intense vibration band at 1381 cm^{-1} can be assigned to the ν_3 mode (asymmetric stretching) of the interlayer carbonate anions [21]. The sharp bands observed at 876 cm^{-1} could be ascribed to mode ν_2 of carbonate anion. Mode ν_4 of carbonate anion could be responsible for bands at 672 cm^{-1} [22]. The lattice stretching and bending vibrations ascribed to O–M and O–M–O bonds are also observed at 785 and 453 cm^{-1}, respectively [23]. The major bands almost vanish after the calcination process, revealing the removal of the anions from the clay interlayer. After the rehydration process, TiO_2/CuMgAl-RLDH sample shows a similar structure with the original LDH, confirming the presence of carbonate anions and small amount of water inside the interlayer space. It is worth mentioning that different bands at 2979, 1091 and 1045 cm^{-1} appear for this rehydration sample. The stronger peak at 2979 cm^{-1} also belongs to the OH stretching mode of interlayer water molecules. However, the action mode is different from the two others. And the weak bands observed at 1091 and 1045 cm^{-1} can be ascribed to the ν_1 mode of carbonate, which is also responsible for the splitting of ν_3 band [24] and this band is IR-inactive in the free carbonate. These results indicate the lower symmetry of carbonate anion in the interlayer of TiO_2/CuMgAl-RLDHs. One of the possible reasons is that the tetravalent titanium cations distributed on the surface of the layer makes a strong electrostatic attraction between the layer and the carbonate anion, influencing the symmetries of the interlayer anions.

The SEM image of LDH precursor (Fig. 4a) illustrates that the CuMgAlTi-LDH is made up of agglomerated platelet-shaped particles with average size of 20–50 nm. It should be mentioned that after calcination the lamellar LDH structure collapses and a solid solution is produced (Fig. 4b) [25]. The SEM image (Fig. 4c) of the resulting RLDH reveals that the LDH structure has been regenerated. Moreover, we note that the hexagonal platelets of the RLDH,

Table 1
Properties of CuMgAlTi-LDH, CuMgAlTi-MMO, and TiO_2/CuMgAl-RLDH.

Sample	d_{003} of LDH (Å)[a]	a of LDH (Å)[a]	Cu/Al molar ratio[b]	Mg/Al molar ratio[b]	Ti/Al molar ratio[b]
CuMgAlTi-LDH	7.48	3.04	0.11	2.69	0.80
CuMgAlTi-MMO	/	/	0.10	2.64	0.73
TiO_2/CuMgAl-RLDH	7.82	3.03	0.11	2.71	0.75

[a] Values determined by XRD.
[b] Amounts of metal elements determined by ICP.

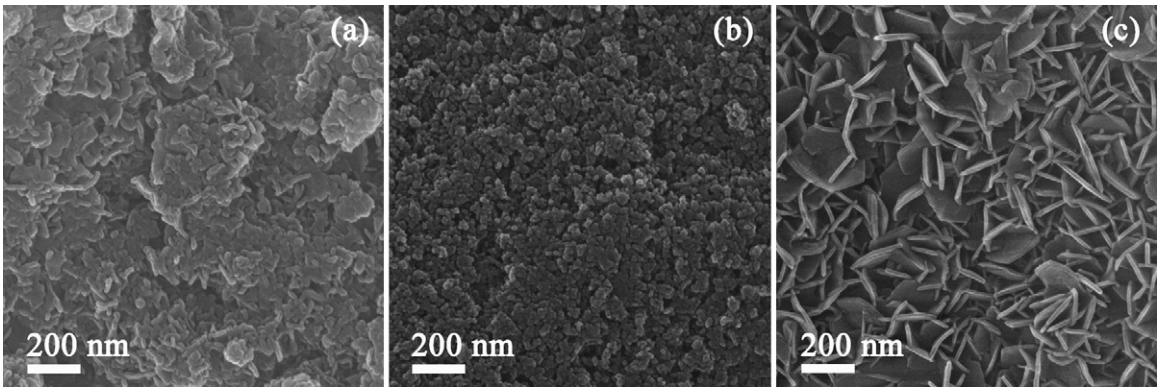

Fig. 4. Representative SEM images of (a) CuMgAlTi-LDH, (b) CuMgAlTi-MMO, and (c) TiO_2/CuMgAl-RLDH.

with particle size above 150 nm, are evolved further after rehydration.

Further structural characterization of TiO_2/CuMgAl-RLDH sample was carried out using TEM image analysis. Fig. 5a shows that TiO_2 nanoparticles are homogeneously dispersed on the surface of the RLDH sample. Fig. 5b and c further exhibit that the TiO_2 particles have a sphere-like shape with an average particle size of 4 nm. The insert of Fig. 5c shows the fast Fourier transform (FFT) analysis of a region of interest. The measurement gives a fringe width of 0.24 nm, which can be attributed to the (0 2 1) basal planes of TiO_2, confirming the presence of anatase-type TiO_2 crystalline. Fig. 5d shows a high magnification view of the selected area enclosed by the black lines of Fig. 5c. The planes with a lattice spacing of about 0.24 nm and 0.26 nm correspond to the (0 2 1) reflection of TiO_2 and the (0 1 2) reflection of LDH, respectively. It can be clearly shown the heterojunction structure on the surface of the TiO_2/CuMgAl-RLDH sample by the HRTEM image.

XPS was utilized to analyze the chemical states of LDH precursor, MMO, and TiO_2/CuMgAl-RLDH. The core level XPS peaks of Cu 2p, Ti 2p, and O 1s for the three samples are shown in Fig. 6. The binding energy of Cu 2p3/2 and 2p1/2 for the LDH precursor are shown at about 932.8 and 954.0 eV, respectively. The two

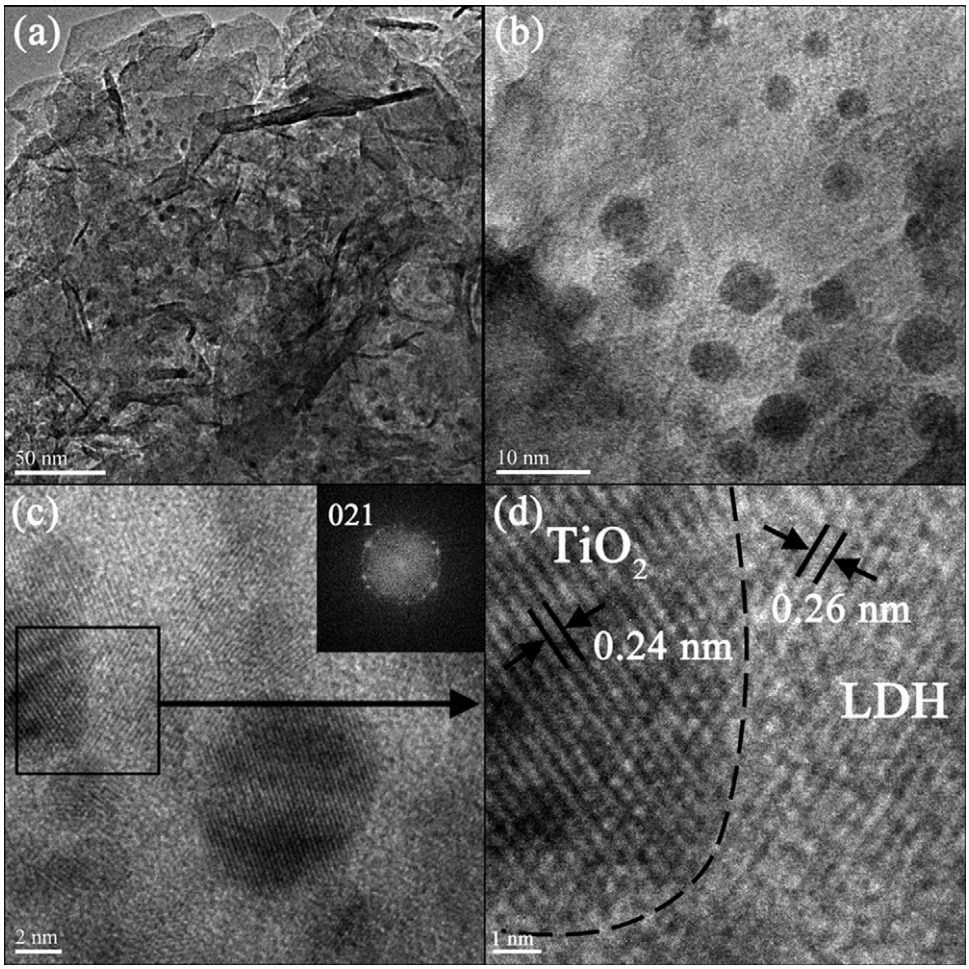

Fig. 5. Representative TEM (a and b) and HRTEM image (c) of TiO_2/CuMgAl-RLDH. (d) Shows high magnification view of the selected area enclosed by the black line of (c). The fast Fourier transform (FFT) analysis of a region of interest is shown as the insert of (c), confirming the presence of anatase-type TiO_2 crystalline.

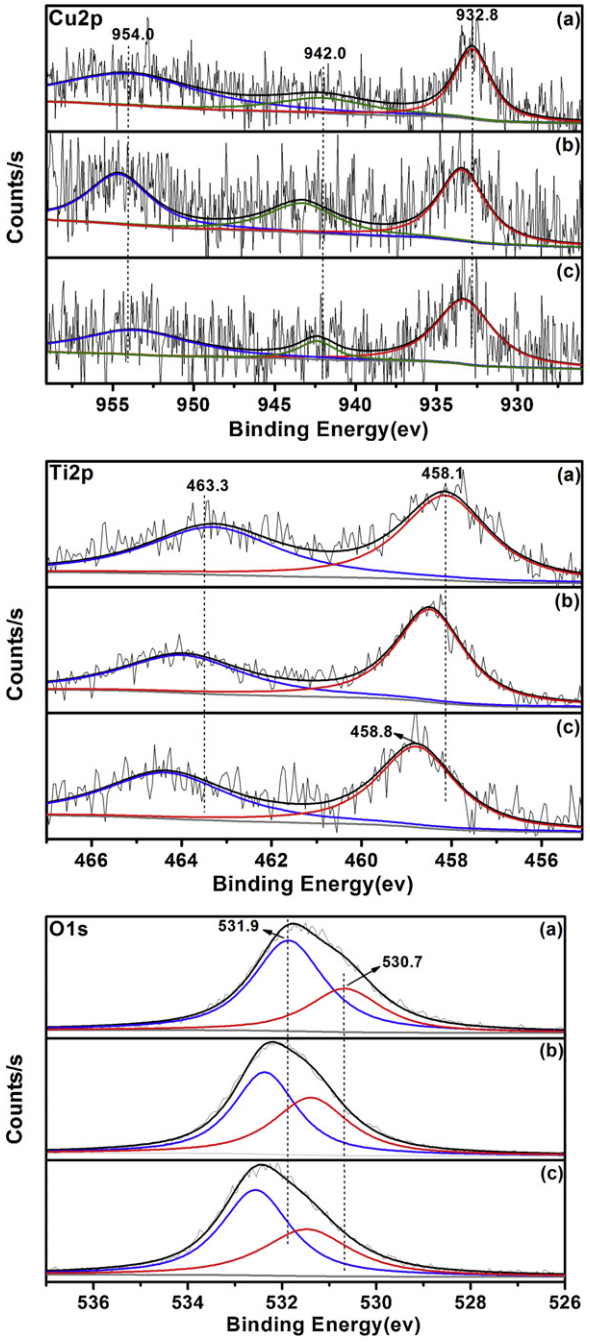

Fig. 6. XPS spectra of (a) CuMgAlTi-LDH, (b) CuMgAlTi-MMO, and (c) TiO_2/CuMgAl-RLDH.

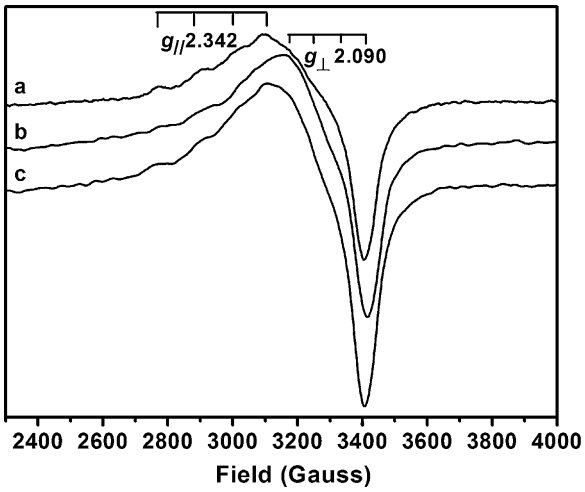

Fig. 7. EPR spectra of (a) CuMgAlTi-LDH, (b) CuMgAlTi-MMO, and (c) TiO_2/CuMgAl-RLDH.

peaks, as well as the shakeup satellite one around 942.0 eV clearly indicate the existence of Cu^{2+} [26,27]. After calcinations, the Cu 2p3/2 and 2p1/2 shift to a higher binding energy. It is noted that after rehydration process, the Cu 2p shift back to a lower binding energy. The binding energy of Cu 2p of the three samples follows in this order: CuMgAlTi-LDH < TiO_2/CuMgAl-RLDH < CuMgAlTi-MMO. A recent solid-state multinuclear magnetic resonance study of LDH [12] revealed that the metal cations within the layers adopt a highly ordered arrangement on an atomic level. Since highly dispersed Cu^{2+} species have lower binding energies than bulk Cu^{2+} in CuO [27], the Cu^{2+} ions may exist in a less dispersed manner after calcination. The subsequent rehydration can result in the regeneration of the ordered arrangement of LDH structure.

As shown in Fig. 6, the binding energy of Ti 2p3/2 and 2p1/2 for the LDH precursor are shown at about 458.1 and 463.3 eV, respectively. Different from that of Cu 2p, the order for binding energy of Ti 2p for the three samples is: CuMgAlTi-LDH < CuMgAlTi-MMO < TiO_2/CuMgAl-RLDH. And, the broad shoulder with binding energy lower than 458.8 eV indicates the existence of Ti in oxidation state lower than 4^+ [28–30], indicating the existing of TiO_2 phase on the surface of TiO_2/CuMgAl-RLDH.

Fig. 6 also displays the O 1s core level spectra for the three samples. It is evident that the signal has been split into two fitted peaks, representing two different kinds of surface species. For the LDH precursor, the first peak (530.7 eV) in lower binding energy could be attributed to the lattice oxygen (O_I) bound to metal cations of the structure, while the second peak (531.9 eV) in higher binding energy could be appearing due to a weak-bonded surface oxygen (O_{II}), including adsorbed oxygen species and mainly hydroxyl groups and O^- (or O_2^{2-}) [31–33]. The binding energy of O 1s for the three samples show in this order: CuMgAlTi-LDH < TiO_2/CuMgAl-RLDH < CuMgAlTi-MMO. Generally, when the energy of an incident light exceeds the band gap of the photocatalyst during the photocatalysis process, the photogenerated electrons combine with adsorbed oxygen to form super oxide anions ($\bullet O_2^-$), and the holes react with OH^- to form hydroxyl radicals ($\bullet$OH) [1]. The photogenerated charge carriers or reactive oxygen species will then react with the reactants. The above order of the binding energy of O 1s indicates that the TiO_2/CuMgAl-RLDH sample may have more advantage as photocatalysts than the LDH precursor.

The EPR spectra for the three samples are presented in Fig. 7. The $g = 2$ regions are contributed by the Cu^{2+} ions [34], exhibiting the anisotropic hyperfine structure in all of the three samples. According to literatures [35–37], the appearing of the well-resolved hyperfine structure on the EPR signals means that Cu^{2+} ions of skeleton are uniformly dispersed in the LDH mainlayer, having a good agreement with the XPS results of Fig. 6. Furthermore, the value for the normal component of g-tensor is found to be $g_{\perp} = 2.090$, and the value for the parallel component of g-tensor $g_{//} = 2.342$, having $A_{//} \approx 100$ G hyperfine splitting. The values of $g_{//}$ and $g_{\perp}$ satisfy the relationship $g_{//} > g_{\perp} > g_e = 2.0023$ (g_e represents the g-factor for a free electron), indicating that the Cu^{2+} ions are coordinated by six ligand atoms in an axially distorted octahedron [38].

It is well known that absorption of light by semiconductors and the migration of the photogenerated electron (e^-) and hole (h^+) pairs are the key factors controlling the photocatalytic behavior of semiconductors. UV–vis absorption measurements are a

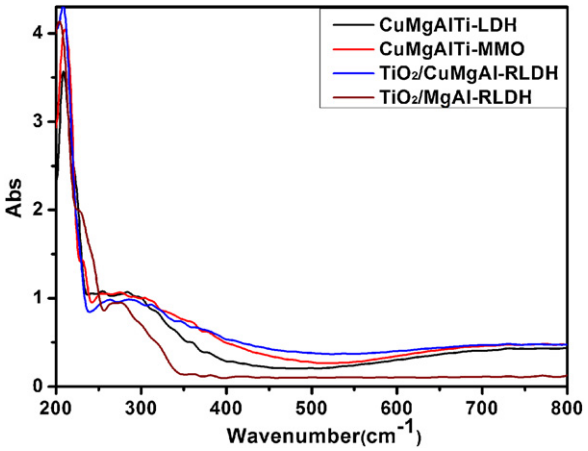

Fig. 8. UV–vis diffuse reflectance spectra of samples.

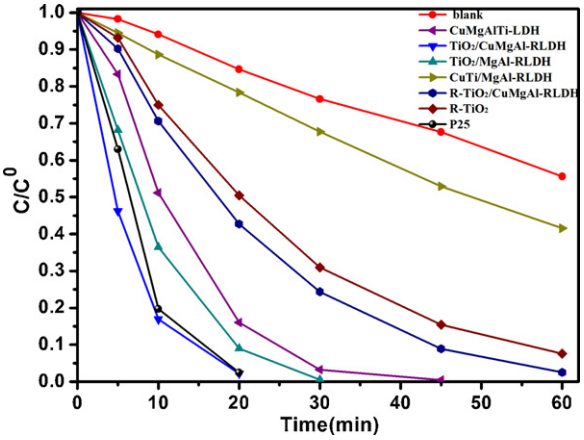

Fig. 10. Photodegradation of MB monitored as the normalized change in concentration as function of irradiation time under UV irradiation.

convenient and effective method for investigating the band structures of semiconductors. As shown in Fig. 8, a noticeable shift of absorption edge to the both UV and visible light regions is observed for the LDH precursor, MMO, and TiO_2/CuMgAl-RLDH. For comparison, the UV–vis absorption of TiO_2/MgAl-RLDH was provided, which shows no absorption in the visible light region. By analysis of the absorption coefficients for these four samples, the so-called optical energy gaps can be estimated using a classical Tauc approach [39,40] as showed in Fig. 9. It has been well established that, for a large number of semiconductors, the dependence of the absorption coefficient α, in the high-frequency region, on the photon energy E_p in optically induced transitions, is given by the following expression:

$$\alpha E_p = K(E_p - E_g)^n \quad (1)$$

where E_g represents the optical band gap, K is a constant, and n depends on the nature of the transition—n has values of 1/2, 3/2, 2, and 3 for allowed direct transitions, forbidden direct transitions, allowed indirect transitions, and forbidden indirect transitions, respectively [41]. In the present case, the best fit of $(\alpha E_p)^2$ versus E_p was obtained for $n = 1/2$, suggesting there are allowed direct transitions across the energy band gap of the samples. The extrapolated value (a straight line to the x-axis) of E_p at $\alpha = 0$ gives absorption edge energies corresponding to E_g. It is worthy noting that the absorption edge of the MMO extends obviously into the visible region, which changed from 3.38 to 2.88 eV. TiO_2/CuMgAl-RLDH extends to a smaller value (2.69 eV) in the visible region. The TiO_2/MgAl-RLDH has a large absorption edge nearly 3.72 eV in the UV region.

Fig. 10 shows the decomposition curves of MB catalyzed by the TiO_2-based samples upon UV exposure. Compared to the CuMgAlTi-LDH precursor, rehydrated TiO_2/CuMgAl-RLDH sample demonstrates a significant enhanced photocatalytic activity that is comparable to Degussa P25, which is consistent with the XPS results (Fig. 6) showing the higher binding energy of O 1s for the TiO_2/CuMgAl-RLDH sample. The photodegradation performance of TiO_2/CuMgAl-RLDH is also compared with rehydrated single phase R-TiO_2, physical mixture of R-TiO_2 and CuMgAl-RLDH (R-TiO_2/CuMgAl-RLDH), composite CuTi/MgAl-RLDH synthesized by the rehydration of mixture of MgAl-MMO and CuTi-MMO, and the TiO_2/MgAl-RLDH without containing Cu ions. Both of the R-TiO_2/CuMgAl-RLDH and CuTi/MgAl-RLDH sample has the same metal elements molar ratio as that of TiO_2/CuMgAl-RLDH sample. Fig. 10 indicates that R-TiO_2, TiO_2/MgAl-RLDH, R-TiO_2/CuMgAl-RLDH, and CuTi/MgAl-RLDH samples exhibit a significant decreased photocatalytic activity.

Fig. 11 shows the degradation curve of MB catalyzed by the samples under visible light irradiation. The corresponding adsorption rate of all samples has been provided in Fig. S1, obviously, except the CuMgAlTi-LDH all of the samples have a very low adsorption capacity after 7 h, indicating the influence of the adsorption capability of the samples on the MB photodegradation test can be ignored. Undoubtedly, Degussa P25, homemade R-TiO_2, and physical mixture R-TiO_2/CuMgAl-RLDH show very weak photocatalytic activity,

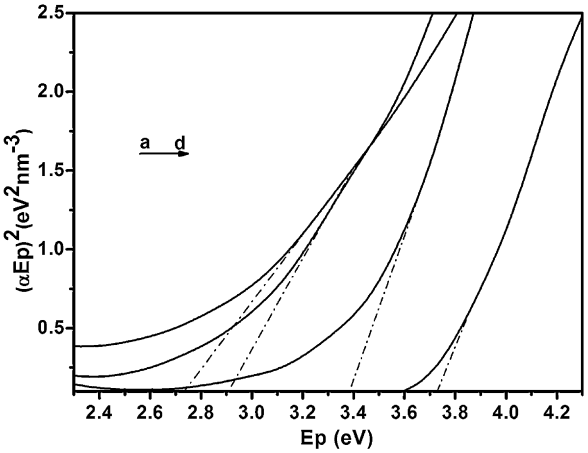

Fig. 9. Tauc plot for (a) TiO_2/CuMgAl-RLDH, (b) CuMgAlTi-MMO, (c) CuMgAlTi-LDH and (d) TiO_2/MgAl-RLDH.

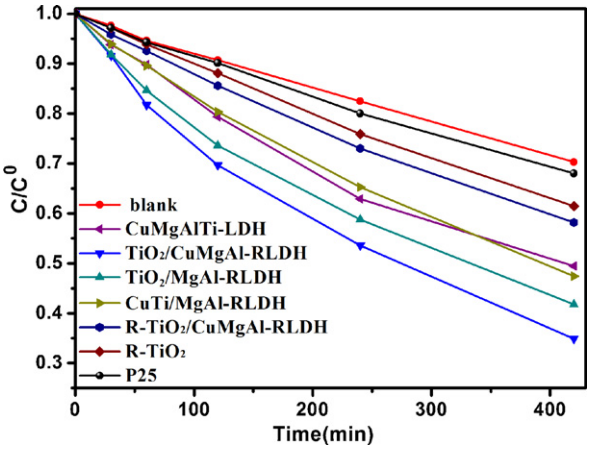

Fig. 11. Photodegradation of MB monitored as the normalized change in concentration as function of irradiation time under visible irradiation.

for the large band gap of TiO_2 semiconductor. It is interesting to note that there are two samples showed unexpected photocatalytic activity under UV and visible light irradiation. One is the CuTi/MgAl-RLDH sample, which exhibits obviously different photocatalytic performance under UV and visible light irradiation. For this sample under UV light irradiation, the doping of bulk CuO in TiO_2 lead to the decreased photocatalytic efficiency, compared to single phase P25 and homemade R-TiO_2 sample. However, under visible light irradiation, CuTi/MgAl-RLDH sample shows a good activity, although lower than TiO_2/CuMgAl-RLDH. The other one is the TiO_2/MgAl-RLDH, which shows good photocatalytic performance both under UV and visible light irradiation. As we know, the visible light does not have enough energy to stimulate TiO_2 generating photoexcited charge carriers. In order to have a better understand of the reaction mechanism, the test on decomposition of formaldehyde was provided. The fact that dyes absorb visible light indicates that a photoreaction might be induced by visible-light photoabsorption (dye sensitization) as well as by photoabsorption of a photocatalyst [42], but the use of formaldehyde as a probe molecule has several merits not only it has no visible light absorption but also the reaction is relatively simple. The measurements and results for photodegradation of formaldehyde have been showed in the electronic supplementary information. From the degradation curve of formaldehyde catalyzed by the TiO_2/CuMgAl-RLDH under visible light irradiation (Fig. S2), we can found that the sample has no photocatalytic activity under visible light irradiation. But under UV light irradiation (Fig. S3), TiO_2/CuMgAl-RLDH also shows better photocatalytic activity than R-TiO_2/CuMgAl-RLDH, CuTi/MgAl-RLDH and TiO_2/MgAl-RLDH. These results indicated that dye sensitization played an important role in the process of photodegradation of MB under visible light irradiation. The good activity of TiO_2/MgAl-RLDH both under UV and visible light irradiation but has no absorption in the visible light regions and the absorption edge was nearly 3.72 eV in the UV region also proved this mechanism. As we known, according to the action spectra of MB decomposition [43], only negligible absorption of MB was observed in the UV region, the MB decomposition in this region can be mainly ascribed to the ordinary band-gap photoexcitation of titania. But in the visible region, MB can absorb photons neither of the photocatalysts. For the CuTi/MgAl-RLDH sample under UV light irradiation, a rapid Cu^{2+} reduction toward Cu^{+} is probably taking place once TiO_2 is photoexcited. The holes left on the valence band of TiO_2 can oxidize hydroxyl to give hydroxyl radicals (•OH), which can degrade the organic pollutants. Since the CuTi/MgAl-RLDH sample has no stabilization of Cu^{+} ion might be considered, a subsequent reoxidation would occur and Cu^{2+} would be formed. Therefore, the existence of Cu^{2+} sites would be considered as recombination centers. But when this sample under visible light irradiation, we postulate that the trapped conduction band electrons may further pass to Cu^{2+} although the formed Cu^{+} ion is not stable for the CuTi/MgAl-RLDH sample, this gives the oxidized dye additional time for electron transfer with MB, thus enabling a second decomposition mechanism. A schematic illustration of the photocatalysis mechanism of CuTi/MgAl-RLDH under irradiation with UV and visible light is shown in Fig. 12b.

Figs. 10 and 11 indicate that TiO_2/CuMgAl-RLDH sample exhibits the highest photocatalytic activity under both UV and visible light irradiation. Zong et al. [44] and Zhang et al. [45] reported the formation of the surface-phase heterojunctions could promote the spatial charge separation in the surface region of TiO_2. The EPR spectra of TiO_2/CuMgAl-RLDH under the irradiation of UV light (λ = 355 nm) showed in Fig. 13. Compared with the spectra in dark, the decrease in intensity for the Cu^{2+} signal upon illumination is due to the trapping of photoexcited electrons in Cu^{2+} sites, forming EPR-silent Cu^{+} sites. Moreover, few changes in the signal intensity of the Ti^{3+} site could be observed, which may be expected to arise

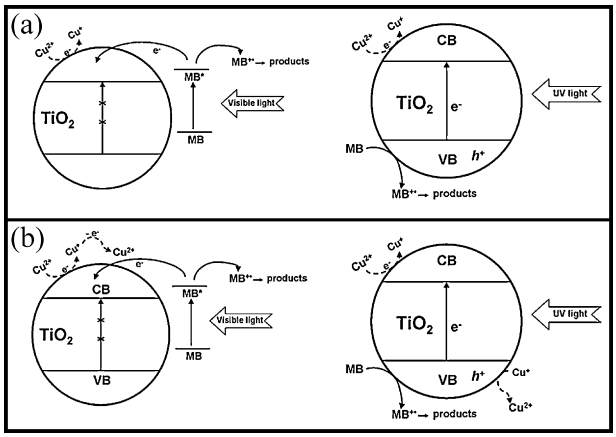

Fig. 12. Schematic illustration of different photocatalysis mechanisms for the photoinduced charge separation in (a) TiO_2/CuMgAl-RLDH and (b) CuTi/MgAl-RLDH under irradiation with UV and visible light.

from the Ti^{4+} site. It is noteworthy that the Cu^{2+} ions can be served as charge trapping sites and thus reduce the recombination rate of the photogenerated e^{-} and h^{+} pairs in the Cu-TiO_2 system [46]. The above EPR result indicates that the photogenerated electrons in the TiO_2/CuMgAl-RLDH quickly transfer from TiO_2 to Cu^{2+}, so that few Ti^{3+} sites could be observed and the intensity of Cu^{2+} signal decreased. Thus, the skeleton Cu^{2+} ions dispersed on the surface of LDH play the role of doping transition metals. The proposed mechanism of the charge generation happening at the heterojunction of the loaded TiO_2 with Cu-incorporated LDH can be explained in Fig. 12a. After the UV light irradiation, the excited electrons from the valence band of TiO_2 transferred to the skeleton Cu^{2+} ions. Consequently, the recombination of an electron and a hole is difficult, as the LDH component captures electrons, increasing the number of holes over the valence band, allowing decomposition to continue. From the above experimental results, we conclude that the formation of the heterojunctions between the TiO_2 nanoparticles and Cu-intercalated LDHs on the surface may be responsible for the high photocatalytic activity of TiO_2/CuMgAl-RLDH. The phase junctions may facilitate transfer of the photogenerated electron from the conduction band of the TiO_2 phase to the trapping sites on the LDHs surface, thereby improving the charge separation efficiency and enhancing the photocatalytic activity.

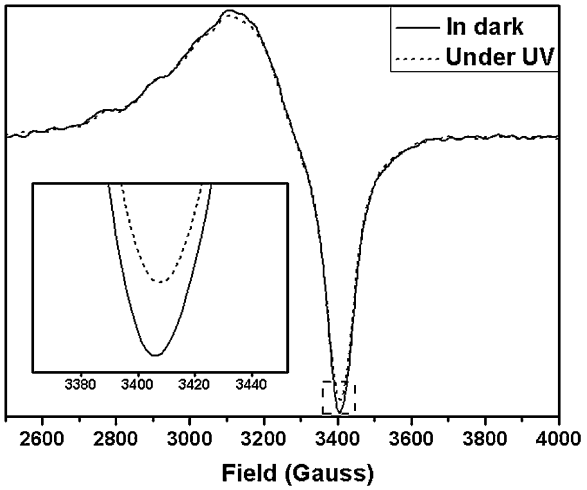

Fig. 13. EPR spectra of TiO_2/CuMgAl-RLDH acquired in dark and under continuous UV light illumination.

4. Conclusions

We have demonstrated that the Cu-doped TiO_2 nanoparticles supported on CuMgAl-LDH can be successfully synthesized based on the characteristic "reconstruction effect" of LDH materials by controlling the rehydration conditions. The Anatase-type TiO_2 nanoparticles are homogeneously distributed on the surface of CuMgAl-RLDH support. The skeleton Cu^{2+} ions dispersed on the surface of LDH can enable the photocatalytic activity, which is markedly higher than those of the rehydrated single phase R-TiO_2, the physical mixture of R-TiO_2 and CuMgAl-RLDH, the composite CuTi/MgAl-RLDH synthesized by the rehydration of mixture of MgAl-MMO and CuTi-MMO, and the TiO_2/MgAl-RLDH prepared under the same procedure as TiO_2/CuMgAl-RLDH without containing Cu ions. The TiO_2/LDH heterojunction nanostructure formed between TiO_2 nanoparticle and LDH support is proposed to contribute the efficient spatial separation between the photogenerated electrons and holes, which can concomitantly improve the photocatalytic activity for TiO_2/CuMgAl-RLDH.

Acknowledgements

We acknowledge generous financial support from the National Natural Science Foundation of China and the 973 Program (No. 2011CBA00506).

Appendix A. Supplementary data

Supplementary data associated with this article can be found, in the online version, at doi:10.1016/j.apcatb.2011.10.022.

References

[1] A.L. Linsebigler, G. Lu, J.T. Yates, Chem. Rev. 95 (1995) 735.
[2] B. O'Regam, M. Gratzel, Nature 353 (1991) 737.
[3] M.A. Fox, M.T. Dulary, Chem. Rev. 93 (1993) 341.
[4] D.H. Kim, H.S. Hong, S.J. Kim, J.S. Song, K.S. Lee, J. Alloys Compd. 375 (2004) 259.
[5] M. Hoffmann, S. Martin, W. Choi, D. Bahnemann, Chem. Rev. 95 (1995) 69.
[6] N. Serpone, D. Lawless, J. Didier, J.M. Herrmann, Langmuir 10 (1994) 643.
[7] Y. Xu, C.H. Langford, J. Phys. Chem. 99 (1995) 11501.
[8] Y. Xu, C.H. Langford, J. Phys. Chem. 101 (1997) 3115.
[9] E.P. Reddy, B. Sun, P.G. Smirniotis, J. Phys. Chem. B 108 (2004) 17198–17205.
[10] V. Rives, Layered Double Hydroxides: Present and Future, Nova Science Publishers, New York, 2001.
[11] G.R. Williams, D. O'Hare, J. Mater. Chem. 16 (2006) 3065–3074.
[12] P.J. Sideris, U.G. Nielsen, Z.H. Gan, C.P. Grey, Science 321 (2008) 113–117.
[13] F. Cavani, F. Trifiró, A. Vaccari, Catal. Today 11 (1991) 173–301.
[14] F. Millange, R.I. Walton, D. O'Hare, J. Mater. Chem. 10 (2000) 1713.
[15] D. Tichit, B. Coq, Cattech 7 (2003) 206.
[16] F. Wong, R.G. Buchheit, Prog. Org. Coat. 51 (2004) 91–102.
[17] J.B. Han, Y.B. Dou, M. Wei, D.G. Evans, X. Duan, Angew. Chem. Int. Ed. 49 (2010) 2171–2174.
[18] I. Pausch, H.H. Lohse, K. Schürmann, R. Allmann, Clays Clay Miner. 34 (1986) 507.
[19] S. Miyata, Clays Clay Miner. 23 (1995) 369.
[20] E.C. Kruissink, L.L. Van Reijden, J.R.H. Ross, J. Chem. Soc. Faraday Trans. 77 (1991) 649.
[21] W. Yang, Y. Kim, P.K.T. Liu, M. Sahimi, T.T. Tsotsis, Chem. Eng. Sci. 57 (2002) 2945–2953.
[22] O. Saber, H. Tagaya, Mater. Chem. Phys. 108 (2008) 449–455.
[23] S.J. Santosa, E.S. Kunarti, Karmanto, Appl. Surf. Sci. 254 (2008) 7612–7617.
[24] N. Nakamoto, Infrared and Raman Spectra of Inorganic and Co-ordination Compounds, fourth ed., John Wiley & Sons, New York, 1986.
[25] J.S. Valente, M.S. Cantú, J.G.H. Cortez, R. Montiel, X. Bokhimi, E.J. Lopez-Salinas, Phys. Chem. C 111 (2007) 642–651.
[26] W. Zhang, Y. Li, S. Zhu, F. Wang, Catal. Today 589 (2004) 93–95.
[27] K.V.R. Chary, G.V. Sagar, C.S. Srikanth, V.V. Rao, J. Phys. Chem. B 111 (2007) 543.
[28] E.C.H. Sykes, M.S. Tikhov, R.M. Lambert, J. Phys. Chem. B 106 (2002) 7290.
[29] J. Abad, C. Rogero, J. Mendez, M.F. Lopez, J.A. Martin-Gago, E. Roman, Surf. Sci. 600 (2006) 2696.
[30] J. Xia, N. Masaki, K. Jiang, S.J. Yanagida, Phys. Chem. B 110 (2006) 25222.
[31] A. Miyakoshi, A. Ueno, M. Ichikawa, Appl. Catal. A 219 (2001) 249–258.
[32] C. Drouet, C. Laberty, J.L.G. Fierro, P. Alphonse, A. Rousset, Int. J. Inorg. Mater. 2 (2000) 419–426.
[33] S.G. Christoskova, M. Stoyanova, M. Georgieva, D. Mehandjiev, Mater. Chem. Phys. 60 (1999) 39–43.
[34] G. Grigoropoulou, K.C. Christoforidis, M. Louloudi, Y. Deligiannakis, Langmuir 23 (2007) 10407–10418.
[35] K. Bahranowski, R. Dula, M. Gasior, M. Labanowska, A. Michalik, L.A. Vartikian, E.M. Serwicka, Appl. Clay Sci. 18 (2001) 93.
[36] D. Sreenivasu, V. Chandramouli, Bull. Mater. Sci. 23 (2000) 281.
[37] F. Ciorcas, S.K. Mendiratta, I. Ardelean, M.A. Valente, Eur. Phys. J. 20 (2001) 235.
[38] K. Bahranowski, R. Dula, M. Labanowska, E.M. Serwicka, Appl. Spectrosc. 50 (1996) 1439.
[39] L. Zou, X. Xiang, J. Fan, F. Li, Chem. Mater. 19 (2007) 6518–6527.
[40] W. Zhao, W.H. Ma, C.C. Chen, J.C. Zhao, Z.G. Shuai, J. Am. Chem. Soc. 126 (2004) 4782–4783.
[41] T. Yamaki, T. Umebayashi, T. Sumita, S. Yamamoto, M. Maekawa, A. Kawasuso, H. Itoh, Nucl. Instrum. Methods Phys. Res. B 206 (2003) 254–258.
[42] B. Ohtani, Chem. Lett. 37 (2008) 216–229.
[43] X.L. Yan, T. Ohno, K. Nishijima, R. Abe, B. Ohtani, Chem. Phys. Lett. 429 (2006) 606–610.
[44] X. Zong, H.J. Yan, G.P. Wu, G.J. Ma, F.Y. Wen, L. Wang, C. Li, J. Am. Chem. Soc. 130 (2008) 7177.
[45] J. Zhang, Q. Xu, Z.C. Feng, M.J. Li, C. Li, Angew. Chem. Int. Ed. 47 (2008) 1766–1769.
[46] X. Li, P.L. Yue, C. Kutal, N. J. Chem. 8 (2003) 1264.